PROCEEDINGS OF SCIENCE

Update on the isospin breaking corrections to the HVP with C−periodic boundary conditions

Anian Altherr,[a] Isabel Campos,[b] Alessandro Cotellucci,[c,d] Roman Gruber,[a] Tim Harris,[a] Javad Komijani,[a] Jens Lücke,[c,e] Marina Krstić Marinković,[a] Letizia Parato,[a,*] Agostino Patella,[c,e] Sara Rosso[b] and Paola Tavella[a]

[a] *Institut für Theoretische Physik, ETH Zürich, Wolfgang-Pauli-Str. 27, 8093 Zürich, Switzerland*

[b] *Instituto de Física de Cantabria and IFCA-CSIC, Avda. de Los Castros s/n, 39005 Santander, Spain*

[c] *Humboldt Universität zu Berlin, Institut für Physik and IRIS Adlershof, Zum Großen Windkanal 6, 12489 Berlin, Germany*

[d] *Jülich Supercomputing Centre, Forschungszentrum Jülich, D-52428 Jülich, Germany*

[e] *DESY, Platanenallee 6, D-15738 Zeuthen, Germany*

E-mail: lparato@phys.ethz.ch

In the RC* collaboration, we simulate lattice QCD+QED using C−periodic spatial boundary conditions to ensure that locality, gauge invariance, and translational invariance are preserved throughout the calculation. We present our progress in computing isospin-breaking (IB) corrections to the leading hadronic contribution to $(g-2)_\mu$. We compare two ways of including the IB corrections: the RM123 method and dynamical QCD+QED simulations, both with C−periodic boundary conditions. The two calculations are performed at $\beta = 3.24$ with four flavours of $O(a)$−improved Wilson fermions; the QCD ensemble features $SU(3)$−symmetric sea quarks plus charm, while down and strange quarks are degenerate in QCD+QED gauge ensembles.

The 41st International Symposium on Lattice Field Theory (LATTICE2024)
28 July - 3 August 2024
Liverpool, UK

*Speaker

1. Introduction

Achieving sub-percent precision in hadronic quantity predictions within lattice QCD requires accounting for isospin-breaking (IB) effects from $m_u \neq m_d$ and from QED, each contributing at the $\sim 1\%$ level. The RC* collaboration has developed a framework using C-periodic boundary conditions [1–4] in lattice ensembles, allowing for a lattice formulation of QCD+QED that preserves locality, gauge invariance, and translational invariance. Consequently, the collaboration focuses primarily on observables where IB effects are significant, such as the measurement of charged meson masses and the hadronic vacuum polarization (HVP) [5, 7–12].

The goal of this preliminary analysis is to compare two methods for computing observables with IB effects, focusing on their relative performance and uncertainties:

1. Monte Carlo sampled, dynamical QCD+QED, where the photon field evolves alongside the SU(3) gauge field in the HMC algorithm. This method requires a setup where $m_u \neq m_d$.

2. The RM123 method [13, 14], applied to an ensemble generated in isospin-symmetric QCD (isoQCD), i.e. with $m_u = m_d$ and $e^2 = 0$.

The observable chosen for this comparison is a_μ^{HVP}, the HVP contribution to $(g-2)_\mu$, for which sub-percent precision—and thus inclusion of IB effects—are currently required [15].

The analysis is performed on ensemble `A380a07b324` ($N_f = 1{+}2{+}1$) for dynamical QCD+QED and ensemble `A400a00b324` ($N_f = 3+1$) for isoQCD+RM123. Both ensembles, generated in Ref. [8] using C* boundary conditions, share the same simulation setup, except for the inclusion of QED and a slightly lighter m_u in `A380a07b324`.

We consider two approaches to compare the results obtained from the two methods above:

(a) Use theoretical, error-free shifts in the bare parameters $\vec{\varepsilon} = (\beta, e^2, m_u, m_d, m_s, m_c)$, defined as $\Delta\vec{\varepsilon} = \vec{\varepsilon}_{\mathrm{A380}} - \vec{\varepsilon}_0$, where $\vec{\varepsilon}_{\mathrm{A380}}$ and $\vec{\varepsilon}_0$ correspond to the parameters of the QCD+QED (`A380a07b324`) and isoQCD (`A400a00b324`) ensembles, respectively. Denoting with $\langle \ldots \rangle_0$ measurements in isoQCD, the shifted quantities $\langle \phi_i(\vec{\varepsilon}_0)\rangle_0 + \Delta\vec{\varepsilon} \cdot \langle \partial_{\vec{\varepsilon}} \phi_i(\vec{\varepsilon}_0)\rangle_0$ can be compared to those measured on the QCD+QED ensemble, $\langle \phi_i(\vec{\varepsilon})\rangle$; a similar comparison applies to the gradient flow scale t_0. Here, ϕ_i refers to combinations of meson masses, as described in Sec. 2.2. This approach allows us to analyze how the uncertainty is distributed between a_μ^{HVP}, the scale-setting parameter t_0, and the tuning observables ϕ_i. Graphically, this comparison corresponds to two points in the ϕ_i, t_0, and a_μ^{HVP} space: one representing the dynamical QCD+QED result and the other the isoQCD+RM123 result, with uncertainties accounted for in all directions.

(b) Compute the shifts $\Delta\vec{\varepsilon} = \vec{\varepsilon}_* - \vec{\varepsilon}_0$ (along with their uncertainties) that solve the renormalization conditions $\langle \phi_i(\vec{\varepsilon}_0)\rangle_0 + \Delta\vec{\varepsilon} \cdot \langle \partial_{\vec{\varepsilon}} \phi_i(\vec{\varepsilon}_0)\rangle_0 = \phi_i^*$, where ϕ_i^* are target, error-free quantities defined as the central values of the observables $\langle \phi_i(\vec{\varepsilon})\rangle$ measured on the QCD+QED ensemble. A similar renormalization condition is applied to the scale-setting observable t_0. This approach transfers all uncertainties to the target observable. On the dynamical QCD+QED side, propagating the uncertainties of ϕ_i to a_μ^{HVP} requires computing $\frac{d}{d\phi_i} a_\mu^{\mathrm{HVP}} = \frac{\partial}{\partial \vec{\varepsilon}} a_\mu^{\mathrm{HVP}} \cdot (\frac{\partial}{\partial \vec{\varepsilon}} \phi_i)^{-1}$, which can be computed directly on `A380a07b324` or approximated using the derivatives computed on the isoQCD ensemble: this should only introduce $O((e^2 + \Delta m_f)^2)$ IB corrections.

In this proceeding, we adopt the first procedure, using error-free bare parameters shifts $\Delta\vec{\varepsilon}$ to compute observables in the isoQCD+RM123 framework. Moreover, we omit valence-disconnected Wick contractions and focus solely on valence-connected ones, while also neglecting IB effects from sea quarks (see Table 3).

2. Setup

This section introduces the C−periodic boundary conditions used in our lattice QCD+QED simulations and outlines the ensembles and renormalization scheme employed in the analysis.

2.1 C−periodic (or C*) Boundary Conditions

Periodic Boundary Conditions (BCs) in finite-volume lattice simulations prevent the propagation of electrically charged states. To overcome this limitation, C-periodic (for brevity, $C^\star$ in the following) BCs were introduced [1, 4]. These boundary conditions allow charged hadrons to propagate in a finite lattice while preserving locality, gauge invariance, and translational invariance [5]. $C^\star$ BCs are imposed by requiring that the gauge field transforms across the boundaries as $U_\mu(x + L_i\hat{i}) = U^*_\mu(x)$, while the fermion fields transform as $\psi(x + L_i\hat{i}) = C^{-1}\bar{\psi}^T(x)$ and $\overline{\psi}(x + L_i\hat{i}) = -\psi^T(x)C$, with C being the charge conjugation matrix and $\hat{i}$ a unit vector in the $i = 1, 2, 3$ spatial directions.

Finite-volume corrections to charged hadron masses exhibit power-law scaling under $C^\star$ BCs. Structure-dependent corrections appear only at $O(1/L^4)$, in contrast to $O(1/L^3)$ in other formulations like QED$_L$, significantly reducing finite-volume effects. $C^\star$ BCs also reduce finite-volume effects to a_μ^{HVP}, with respect to periodic BCs [6].

A consequence of imposing $C^\star$ BCs is a weak violation of flavor conservation, as flavor-charged particles traveling around the torus transform into their antiparticles. However, this effect is exponentially suppressed with volume and is negligible for practical purposes in numerical simulations [5].

2.2 Ensembles

Table 1 lists the simulation parameters $\vec{\varepsilon}_0$ and $\vec{\varepsilon}_{\text{A380}}$ for the isoQCD (`A400a00b324`) and QCD+QED (`A380a07b324`) ensembles, while Table 2 defines their renormalization scheme.

In the isoQCD setup, where $m_u = m_d = m_s$, there are only two distinct light meson masses: $M_{\pi^\pm} = M_{K^\pm} = M_{K^0} = 398.5(4.7)$ MeV and $M_{D^\pm} = M_{D_s^\pm} = M_{D^0} = 1912.7(5.7)$ MeV. This symmetry significantly reduces the number of meson mass derivatives required for the RM123 method. For comparison, the QCD+QED ensemble yields $M_{\pi^\pm} = M_{K^\pm} = 383.6(4.4)$ MeV, $M_{K^0} = 390.7(3.7)$ MeV, $M_{D^\pm} = M_{D_s^\pm} = 1926.4(7.8)$ MeV, and $M_{D^0} = 1921.1(7.6)$ MeV, as previously computed in Ref. [8].

2.3 RM123: Feynman diagrams with our action and vector currents

For this analysis, we use both local-local and conserved-local implementations of the vector current correlator $G(t)$, defined in Section 4. As a result, the leading IB effects arise from two sources: the action and the conserved current V^c_μ at the sink, where the action is described in

Ensemble	lattice	β	α	κ_u	$\kappa_d = \kappa_s$	κ_c
A400a00b324	64×32^3	3.24	0	0.13440733	0.13440733	0.12784
A380a07b324	64×32^3	3.24	0.007299	0.13459164	0.13444333	0.12806355
		$\Delta\beta$	$\Delta\alpha$	Δm_u	$\Delta m_d = \Delta m_s$	Δm_c
		0	0.007299	-0.00509422	-0.000996117	-0.00682735

Table 1: Parameters of the isoQCD (first row) and QCD+QED (second row) ensembles. The isoQCD ensemble has $\kappa_u = \kappa_d = \kappa_s$, while the QCD+QED ensemble has $\kappa_u > \kappa_d = \kappa_s$ to account for $m_u < m_d$, with degenerate down and strange quarks. The parameter shifts $\Delta\varepsilon_k$ for β, $\alpha = 4\pi e^2$, and quark masses are listed at the bottom of the table. These shifts can be extracted directly since both lattices use the same simulation code and action.

Observable	Physical value	RC* target value		Measured Values	
		isoQCD	QCD+QED	isoQCD	QCD+QED
$\phi_0 = 8t_0(m^2_{K^\pm} - m^2_{\pi^\pm})$	0.992	0	0	—	—
$\phi_1 = 8t_0(m^2_{K^\pm} + m^2_{\pi^\pm} + m^2_{K^0})$	2.26	2.11	2.11	2.107(50)	1.977(37)
$\phi_2 = 8t_0(m^2_{K^0} - m^2_{K^\pm})/\alpha_R$	2.36	0	2.36	—	3.39(14)
$\phi_3 = \sqrt{8t_0}(m_{D_s^\pm} + m_{D^0} + m_{D^\pm})$	12.0	12.1	12.1	12.068(36)	12.132(48)
$\sqrt{8t_0}$ / fm	0.415	0.415	0.415		
α_R	0.007297	0	α^{phys}		

Table 2: Renormalization scheme for isoQCD (`A400a00b324`) and QCD+QED (`A380a07b324`) ensembles, generated in [8]. The scale is set using $\sqrt{8t_0} = 0.415$ fm from Ref. [20], giving lattice spacings $a = 0.05393(24)$ fm (isoQCD) and $a = 0.05323(28)$ fm (QCD+QED). Physical values of $\phi_{0,1,2,3}$ are compiled using the experimental masses in [21], without errors. At leading order in ChPT, ϕ_i depend on quark mass combinations: $\phi_0 \propto (m_s - m_d)$, $\phi_1 \propto (m_u + m_d + m_s)$, $\phi_2 \propto (m_u - m_d)$, and $\phi_3 \propto m_c$.

detail in the `openQCD` and `openQxD` documentations [16–19]. Table 3 provides a summary of all Feynman diagrams at first order in Δm_f and e^2 which are required to compute the IB corrections to $G(t)$. The diagrams are categorized by valence quark connections (connected or disconnected) and by the placement of IB insertions on valence, sea, or mixed quarks. Note that for $m_d = m_s$, the "U-isovector" current $\bar\psi_d\gamma_\mu\psi_d - \bar\psi_s\gamma_\mu\psi_s$ requires no valence-disconnected diagrams, as these cancel by d-s symmetry. This quantity will be the focus of future work.

3. Scheme matching and mass parameter shifts

The Eqs. (1a)-(1d) provide the first-order expansions (denoted by superscript $^{(1)}$) in the bare parameters e^2 and Δm_f for the scheme-defining observables ϕ_i defined in Table 2:

$$\phi_0^{(1)} = \phi_0^{(0)} = 0\,, \tag{1a}$$

$$\begin{aligned}\phi_1^{(1)} = \phi_1^{(0)} + 16t_0^{(0)} m_{\pi^\pm}^{(0)} \Big[\Big(\sum\nolimits_{f=d,s} \Delta m_f (\partial_{m_f} m_{K^0})^{(0)} + e^2 (\partial_{e^2} m_{K^0})^{(0)} \Big) \\ + 2 \Big(\sum\nolimits_{f=u,d} \Delta m_f (\partial_{m_f} m_{\pi^\pm})^{(0)} + e^2 (\partial_{e^2} m_{\pi^\pm})^{(0)} \Big) \Big]\,,\end{aligned} \tag{1b}$$

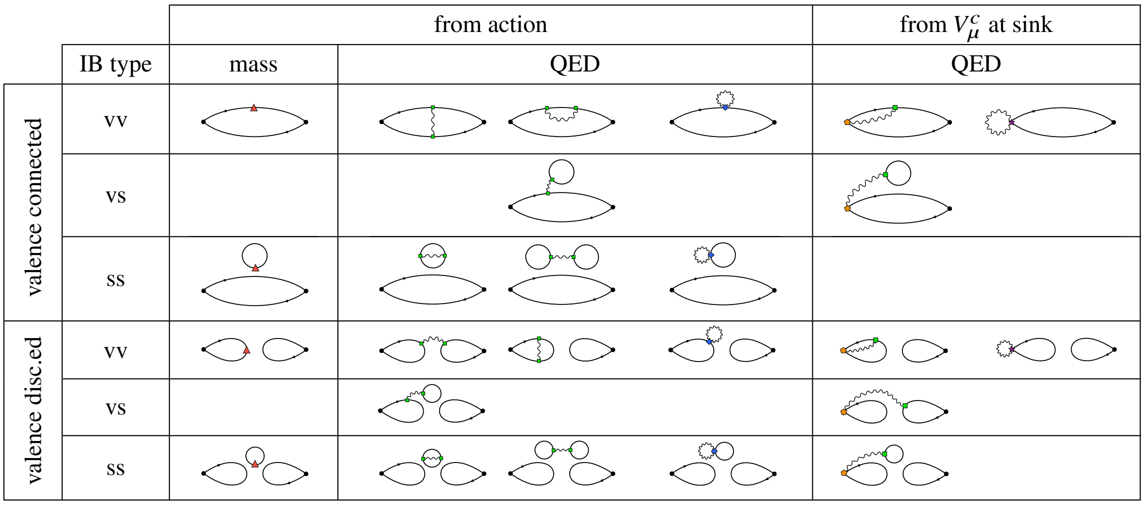

Table 3: Diagrams of IB contributions to a two-point function, in mass and QED sectors. Colored symbols denote operator insertions: red triangle (mass term, $\sum_x \bar\psi_f\psi_f$), green square (single photon insertion, from either $\partial_e D_W$ or $\partial_e D_{SW}$), blue diamond (photon tadpole, from $\partial_e^2 D_W$ only, because $\partial_e^2 D_{SW} = 0$). When using conserved-local correlator $G^{cl}(t)$, and thus conserved vector current V_k^c at sink, additional insertions appear (last column): orange pentagon (single photon, from $\partial_e V_k^c(0)$) and purple star (tadpole, from $\partial_e^2 V_k^c(0)$). Only vv-IB corrections to valence-connected diagrams (first row, top block) are included in this analysis, neglecting disconnected diagrams (bottom block) and sea quark contributions (vs, ss rows).

$$\phi_2^{(1)} = \phi_2^{(0)} + 16t_0^{(0)} \frac{m_{K^0}^{(0)}}{4\pi e^2}\Big[\Big(\sum_{f=d,s} \Delta m_f (\partial_{m_f} m_{K^0})^{(0)} + e^2(\partial_{e^2} m_{K^0})^{(0)}\Big) - \Big(\sum_{f=u,s} \Delta m_f (\partial_{m_f} m_{K^\pm})^{(0)} + e^2(\partial_{e^2} m_{K^\pm})^{(0)}\Big)\Big], \tag{1c}$$

$$\phi_3^{(1)} = \phi_3^{(0)} + \sqrt{8t_0^{(0)}}\Big[\Big(\sum_{f=u,c} \Delta m_f (\partial_{m_f} m_{D^0})^{(0)} + e^2(\partial_{e^2} m_{D^0})^{(0)}\Big) + 2\Big(\sum_{f=d,c} \Delta m_f (\partial_{m_f} m_{D^\pm})^{(0)} + e^2(\partial_{e^2} m_{D^\pm})^{(0)}\Big)\Big], \tag{1d}$$

where $X^{(0)}$ indicates that the observable X is defined and computed in isoQCD. The derivatives of scale t_0 are currently ignored and will be included alongside the IB effects from sea quarks. For the same reason, the additional equation for the lattice spacing, $a = a^{(0)} - \frac{1}{2}(\Delta\hat t_0/\hat t_0)\, a^{(0)}$, where $\Delta\hat t_0 = \sum_f \Delta m_f(\partial_{m_f}\hat t_0)^{(0)} + e^2(\partial_{e^2}\hat t_0)^{(0)} + \Delta\beta(\partial_\beta \hat t_0)^{(0)} = 0$, is also neglected. Moreover, in our isoQCD setup, several mass degeneracies occur, due to $m_u = m_d = m_s$; in particular $K^\pm$ and $\pi^\pm$ are effectively the same particle, similarly for $D_s^\pm = D^\pm$. These degeneracies have been used to simplify several terms in Eqs. (1a)-(1d).

If we were to pursue strategy (b) described in Section 1, we would need to fix the left-hand side of Eqs. (1a)-(1d) to the target QED+QCD scheme and compute the mass shifts Δm_f that satisfy the system of equations. Since we are here following strategy (a), we fix Δm_f to the values given in Table 1 and compute the set of ϕ_i for isoQCD+RM123 with their errors:

$$\phi_1 = 2.164(23)(4)\,, \quad \phi_2 = 3.602(47)(27)\,, \quad \phi_3 = 12.095(30)(1)\,, \tag{2}$$

where the first and second brackets correspond to the statistical and systematic errors, respectively. These values can be compared to those computed directly on the `A380a07b324` ensemble.

PoS(LATTICE2024)119

4. a_μ^{HVP} in QCD+QED

The HVP contribution to the $(g-2)$ of the muon, a_μ^{HVP}, is given by:

$$a_\mu^{\mathrm{HVP}} = \left(\frac{\alpha}{\pi}\right)^2 \sum_{f_1,f_2} \int_0^\infty dt\, G^{R,ll}_{f_1 f_2}(t) K(t;m_\mu), \tag{3}$$

where $G_{f_1 f_2}(t) = q_{f_1} q_{f_2} \frac{1}{3}\sum_{k=1}^{3}\sum_{\vec{x}} \langle V_k^{f_1}(x) V_k^{f_2}(0)\rangle$, with $V_k^{f_1}(x)$ the vector current, and $K(t;m_\mu)$ defined as in Ref. [22, Eq. 44]. Here, $G^{R,ll}(t)$ represents the renormalized local-local correlator $G^{R,ll}(t) = Z_V G^{ll}(t) Z_V^T$, where G and Z_V are 4×4 matrices in the flavor basis (see [23] for the renormalization pattern with $N_f = 3$, $O(a)$-improved Wilson fermions). The computation of Z_V is briefly discussed in Sec. 4.1.

Alternatively, we use the renormalized conserved-local correlator $G^{R,cl}(t) = Z_V G^{cl}(t)$.

The IB corrections to a_μ^{HVP} are categorized into two main types:

1. Corrections to correlators:

$$\delta_G a_\mu^{\mathrm{HVP}} = \left(\frac{\alpha}{\pi}\right)^2 \int dt\, Z_V^{(0)} \Delta G^{ll}(t) Z_V^{(0)^T} K(t;m_\mu) \tag{4}$$

$$\Delta G^{ll}(t) = \sum_f \Delta m_f \left(\frac{\partial G^{ll}(t)}{\partial m_f}\right)^{(0)} + e^2 \left(\frac{\partial G^{ll}(t)}{\partial e^2}\right)^{(0)} \tag{5}$$

2. Corrections to renormalization constants:

$$\delta_Z a_\mu^{\mathrm{HVP}} = \left(\frac{\alpha}{\pi}\right)^2 \int dt\, \left[Z_V^{(0)} G^{ll}(t)^{(0)} \Delta Z_V^T + \Delta Z_V G^{ll}(t)^{(0)} Z_V^{(0)^T}\right] K(t;m_\mu) \tag{6}$$

$$\Delta Z_V = \sum_f \Delta m_f \left(\frac{\partial Z_V}{\partial m_f}\right)^{(0)} + e^2 \left(\frac{\partial Z_V}{\partial e^2}\right)^{(0)} \tag{7}$$

If sea-sea effects were included, the IB corrections to the lattice spacing would also require considering the derivative of the kernel with respect to a, due to its implicit dependence $t = a\hat{t}$.

4.1 Renormalization constants Z_V at leading order

The renormalization conditions are defined in the adjoint basis of SU(4) generators $\lambda_3, \lambda_8, \lambda_{15}$, and the identity $\lambda_0 = \mathbb{1}$ as outlined in Refs. [23, 24]:

$$V_\mu^{em} = \sum_{f=u,d,s,c} Q_f \bar{\psi}_f \gamma_\mu \psi_f = \frac{1}{3} V_\mu^0 + V_\mu^3 + \frac{1}{\sqrt{3}} V_\mu^8 - \frac{1}{\sqrt{6}} V_\mu^{15} \tag{8}$$

where the adjoint currents are $V_\mu^{0,3,8} = \frac{1}{2}\mathrm{tr}(\lambda_{0,3,8}\mathcal{V})$ and $V_\mu^{15} = \mathrm{tr}(\lambda_{15}\mathcal{V})$, with $[\mathcal{V}]_{f_1 f_2} = \bar{\psi}_{f_1}\gamma_\mu\psi_{f_2}$. In the adjoint basis, we define $\tilde{Z}_V$ as follows:

$$\left[\tilde{Z}_V\right]_{ab} = \lim_{x_0\to\infty} \tilde{G}^{cl}_{ad} \cdot (\tilde{G}^{ll})^{-1}_{db}, \quad a,b = 0,3,8,15. \tag{9}$$

In this work, we are neglecting the disconnected terms. As a consequence, the renormalization constant matrices, when brought back in the flavor bases, are diagonal and computed to be:

$$Z_V^{A400} = \mathrm{diag}(0.6771(3),\ 0.6771(3),\ 0.6771(3),\ 0.6050(8))\,, \tag{10}$$

$$Z_V^{A380} = \mathrm{diag}(0.6775(6),\ 0.6793(7),\ 0.6793(7),\ 0.6048(9))\,. \tag{11}$$

4.2 Leading-order results for $a_\mu^{\rm HVP}$ from connected correlators

Results for $a_\mu^{\rm HVP}$ from leading-order (LO) connected correlators are given in columns 1 and 3 of Table 5 (Conclusions) for ensembles `A400a00b324` and `A380a07b324`. Here "leading-order" is used to indicate 2-point functions only, rather than QCD only, as QED effects are inherently included in the QCD+QED ensemble `A380a07b324`.

All calculations were performed using 2000 configurations with 4 point sources per configuration, neglecting disconnected contributions. At large Euclidean times, the correlator tails were reconstructed using single-exponential fits with $t_{\rm cut} \in (1.2, 1.3)$ fm.

4.3 Corrections from derivatives of correlator

The derivatives $\partial_{m_f} G(t)$ and $\partial_e^2 G(t)$ correspond, diagrammatically, to the first row of Table 3, neglecting disconnected and sea effects. The $O(e^2)$ insertions come from derivatives of the Wilson-Dirac operator $D_{\rm W}$ and the Sheikholeslami–Wohlert (SW) term $\delta D_{\rm SW}$ in the Dirac operator [19, Eqs. 8, 10, 13], leading to a total of 8 Wick contractions (11 for conserved-local) for each flavor.

The corrections to the tail parameters A and $m_{\rm eff}$ are defined as $A = A^{(0)} + \Delta A$ and $m_{\rm eff} = m_{\rm eff}^{(0)} + \Delta m_{\rm eff}$. The parameters ΔA and $\Delta m_{\rm eff}$ are extracted from a two-parameter linear fit:

$$\frac{G^{(1)}(x_0) - G^{(0)}(x_0)}{G^{(0)}(x_0)} = \frac{\Delta A}{A^{(0)}} - x_0 \Delta m_{\rm eff}. \tag{12}$$

To estimate systematic effects, this procedure is repeated over different fit ranges for the light quarks.

4.4 Corrections from derivatives of Z_V

The correction to Z_V are defined in Eq. (7). We expect $\delta_{Z_V} a_\mu^{\rm HVP}$ in the case of local-local discretization to be approximately twice as large as the corresponding correction in the conserved-local case, provided that $a_\mu^{\rm HVP}$ from both cl and ll prescriptions agree at leading order.

The Wick contractions needed to compute $\partial_{\varepsilon_i} Z_V$ are the same as those for $\partial_{\varepsilon_i} G(x_0)$. These are fitted to the following expression, derived from Eq. (9):

$$\frac{\partial Z_{V_R V_l}}{\partial \varepsilon_i} = \lim_{x_0 \to \infty} \left[\frac{\partial G^{cl}}{\partial \varepsilon_i}(x_0) - G^{cl}(x_0) \left(G^{ll}(x_0)\right)^{-1} \frac{\partial G^{ll}}{\partial \varepsilon_i}(x_0) \right] \cdot \left(G^{ll}(x_0)\right)^{-1}. \tag{13}$$

Tables 4 and 5 summarize IB corrections and total $a_\mu^{\rm HVP}$, respectively. Results for the total $a_\mu^{\rm HVP}$ are provided for the QCD+QED and isoQCD+RM123 setups, as well as for the isoQCD case.

5. Outlook and Conclusions

This work compares two methods for computing IB effects to the HVP, including all valence-connected terms. Sea-valence and sea-sea IB effects, yet to be added, are computed on the same ensemble `A400a00b324`. A discussion of these effects, restricted to the $N_f = 3$ case, is contained in Ref. [25]. Results from isoQCD+RM123 and dynamical QCD+QED (Table 5) show slight incompatibility, underscoring the importance of sea IB effects to achieve full consistency.

Future work will use the isovector current $\bar{d}\gamma_\mu d - \bar{s}\gamma_\mu s$, which is well-defined and free of disconnected diagrams. The initial analysis will focus on the intermediate time window and omit reconstruction of the long-distance piece.

PoS(LATTICE2024)119

Corrections from renormalization constants $\times 10^{10}$				
ll	$\delta_{Z_v} a_\mu^{uu}$	$-510(33)\Delta m_u - 22(3)e^2$	$2.60(17) - 2.02(28)$	$0.58(44)$
	$\delta_{Z_v} a_\mu^{dd}$	$0.016(23)\Delta m_u - 128(8)\Delta m_d - 1.4(2)e^2$	$0.127(8) - 0.128(18)$	$0.001(26)$
	$\delta_{Z_v} a_\mu^{cc}$	$0.003(4)\Delta m_u - 6.37(2)\Delta m_c - 0.578(2)e^2$	$0.04347(14) - 0.05302(18)$	$-0.00954(34)$
cl	$\delta_{Z_v} a_\mu^{uu}$	$-252(16)\Delta m_u - 11(2)e^2$	$1.28(8) - 1.01(18)$	$0.27(26)$
	$\delta_{Z_v} a_\mu^{dd}$	$0.008(11)\Delta m_u - 63(4)\Delta m_d - 0.68(11)e^2$	$0.063(4) - 0.062(10)$	$0.000(14)$
	$\delta_{Z_v} a_\mu^{cc}$	$0.0012(16)\Delta m_u - 2.516(9)\Delta m_c - 0.228(8)e^2$	$0.01717(6) - 0.0209(7)$	$-0.0038(1)$
Corrections from correlator $\times 10^{10}$				
ll	$\delta_G a_\mu^{uu}$	$-4364(266)\Delta m_u - 216(14)e^2$	$22.2(1.4) - 19.8(1.3)$	$2.4(2.6)$
	$\delta_G a_\mu^{dd}$	$-1091(67)\Delta m_d - 13.5(9)e^2$	$1.09(7) - 1.24(8)$	$-0.15(15)$
	$\delta_G a_\mu^{cc}$	$-59.2(3)\Delta m_c - 3.119(13)e^2$	$0.404(20) - 0.2861(12)$	$0.118(22)$
cl	$\delta_G a_\mu^{uu}$	$-4591(288)\Delta m_u - 227(15)e^2$	$23.4(1.5) - 20.8(1.4)$	$2.6(2.8)$
	$\delta_G a_\mu^{dd}$	$-1148(72)\Delta m_d - 14.2(1.0)e^2$	$1.14(7) - 1.30(9)$	$-0.16(16)$
	$\delta_G a_\mu^{cc}$	$-57.2(2)\Delta m_c - 3.295(14)e^2$	$0.391(14) - 0.3022(13)$	$0.088(15)$

Table 4: IB corrections from the renormalization constant Z_V and the correlator G, for local-local (ll) and conserved-local (cl) currents. Due to d-s flavor symmetry ($\Delta m_d = \Delta m_s$), d can represent either strange or down quarks. The last column sums the second-to-last column with fully correlated errors: these values are provided as reference, but are not directly added to isoQCD results in Table 5; see its caption for details.

	isoQCD		isoQCD+RM123		QCD+QED	
	ll	cl	ll	cl	ll	cl
$a_\mu^u \times 10^{10}$	188.5(1.9)	186.5(2.0)	192.4(2.0)	189.2(2.0)	194.0(2.3)	192.2(2.2)
$a_\mu^{d/s} \times 10^{10}$	47.1(5)	46.6(5)	47.0(5)	46.4(5)	47.2(6)	46.8(6)
$a_\mu^c \times 10^{10}$	7.59(3)	5.99(3)	7.73(3)	6.07(3)	7.55(4)	5.95(4)

Table 5: Results for a_μ^{HVP} in three setups: isoQCD (left) and two methods for including QED effects: isoQCD+RM123 (center) and dynamical QCD+QED (right). Results for isoQCD+RM123 are not obtained by simply adding IB corrections from Table 4 to the isoQCD results. Instead, consistent fit ranges and tail reconstructions are used across isoQCD and IB corrections, ensuring all correlations are properly handled.

This comparison is a first step towards a systematic comparison of the dynamical QCD+QED approach and perturbative treatment of IB corrections; a final answer will require a variety of observables and ensembles with smaller pion masses, larger volumes, and finer lattice spacings.

Acknowledgments

We acknowledge access to Piz Daint at the Swiss National Supercomputing Centre (CSCS) (projects eth8 and s1196) and to Lise and Emmy at NHR@ZIB and NHR@Göttingen as part of the NHR infrastructure (projects bep00085 and bep00102). Funding from SNSF Project No. 200021_200866 and German Research Foundation (DFG) via Project No. 417533893/GRK2575 "Rethinking Quantum Field Theory" is gratefully acknowledged. This research was supported in part by grant NSF PHY-2309135 to the Kavli Institute for Theoretical Physics (KITP).

PoS(LATTICE2024)119

References

[1] A. S. Kronfeld and U. J. Wiese, *SU(N) gauge theories with C periodic boundary conditions. 2. Small volume dynamics*, *Phys. Rev. D* **93** (1993) 190, [hep-lat/9210008].

[2] Jong-Wan Lee and Brian C. Tiburzi, *Finite Volume Corrections to the Electromagnetic Mass of Composite Particles*, *Phys. Rev. D* **93** (2016) 034012, [1508.04165].

[3] M. Lüscher, *Volume Dependence of the Energy Spectrum in Massive Quantum Field Theories. 1. Stable Particle States*, *Commun. Math. Phys.* **104** (1986) 177.

[4] L. Polley, *Boundaries for $SU(3)_c \times U(1)_{el}$ lattice gauge theory with a chemical potential*, *Z. Phys. C* **59** (1993) 105.

[5] B. Lucini, A. Patella, A. Ramos and N. Tantalo, *Charged hadrons in local finite-volume QED+QCD with C⋆ boundary conditions*, *JHEP* **02** (2016) 076, [1509.01636].

[6] S. Martins and A. Patella, *Finite-Size Effects of the HVP Contribution to the Muon $g-2$ with C⋆ Boundary Conditions*, *PoS* **LATTICE2022** (2023) 323, [2212.09565].

[7] I. Campos *et al.* (RC⋆), *openQ*D code: a versatile tool for QCD+QED simulations*, *Eur. Phys. J. C* **80** (2020) 195, [1908.11673].

[8] L. Bushnaq *et al.* (RC⋆), *First results on QCD+QED with C⋆ boundary conditions*, *JHEP* **03** (2023) 012, [2209.13183].

[9] A. Altherr *et al.* (RC⋆), *Tuning of QCD+QED simulations with C⋆ boundary conditions*, *PoS* **LATTICE2022** (2023) 259, [2212.10894].

[10] A. Altherr *et al.* (RC⋆), *Strange and charm contributions to the HVP from C⋆ boundary conditions*, *PoS* **LATTICE2022** (2023) 281, [2301.04385].

[11] M. E. B. Dale *et al.* (RC⋆), *Baryon masses from full QCD+QED$_C$ simulations*, *PoS* **LATTICE2021** (2022) 373, [2112.12767].

[12] J. Lücke *et al.* (RC⋆), *$N_f = 1+2+1$ QCD+QED simulations with C⋆ boundary conditions*, *PoS* **LATTICE2022** (2023) 064, [2212.09578].

[13] G. M. de Divitiis, P. Dimopoulos, R. Frezzotti, V. Lubicz, G. Martinelli, R. Petronzio, G. C. Rossi, *Lattice QCD calculation of strong isospin breaking effects*, *PoS* **LATTICE2021** (2022) 290, [1202.5222].

[14] G. M. de Divitiis *et al.* (RM123), *Leading isospin breaking effects on the lattice*, *Phys. Rev. D* **87** (2013) 114505, [1303.4896].

[15] T. Aoyama *et al.*, *The anomalous magnetic moment of the muon in the Standard Model*, *Phys. Rept.* **887** (2020) 1, [2006.04822].

[16] M. Lüscher, *Gauge actions in openQCD simulations*, openQCD *documentation* (2013).

[17] M. Lüscher, *Implementation of the lattice Dirac operator*, openQCD *documentation* (2016).

[18] A. Patella, *Gauge actions*, openQxD *documentation* (2017).

[19] A. Patella, *Dirac operator*, openQxD *documentation* (2017).

[20] M. Bruno, T. Korzec and S. Schaefer, *Setting the scale for the CLS* $2+1$ *flavor ensembles*, *Phys. Rev. D* **95** (2017) 074504, [1608.08900].

[21] S. Navas *et al.* (Particle Data Group), *Review of particle physics*, *Phys. Rev. D* **110** (2024) 030001.

[22] M. Della Morte, A. Francis, V. Gülpers, G. Herdoíza, G. von Hippel, H. Horch, B. Jäger, H. B. Meyer, A. Nyffeler, H. Wittig, *The hadronic vacuum polarization contribution to the muon* $g-2$ *from lattice QCD*, *JHEP* **10** (2017) 020, [1705.01775].

[23] A. Gérardin, M. Cè, G. von Hippel, B. Hörz, H. B. Meyer, D. Mohler, K. Ottnad, J. Wilhelm, and H. Wittig, *The leading hadronic contribution to* $(g-2)_\mu$ *from lattice QCD with* $N_\mathrm{f}=2+1$ *flavours of* $O(a)$ *improved Wilson quarks*, *Phys. Rev. D* **100** (2019) 014510, [1904.03120].

[24] T. Bhattacharya, R. Gupta, W. Lee, S. R. Sharpe, and J. M. S. Wu, *Improved bilinears in lattice QCD with non-degenerate quarks*, *Phys. Rev. D* **73** (2006) 034504, [hep-lat/0511014].

[25] A. Cotellucci *et al.* (RC*), *Error Scaling of Sea Quark Isospin-Breaking Effects*, *PoS* **LATTICE2024** (2025) 116.